J Fail. Anal. and Preven. (2020) 20:159–172
https://doi.org/10.1007/s11668-020-00808-x

TECHNICAL ARTICLE—PEER-REVIEWED

Electrochemical Inhibitory Effects of Non-edible Vegetable Oils on Low-Alloyed Low Carbon Steel in H_2SO_4

Olanrewaju M. Adesusi · Olayide R. Adetunji · Salami O. Ismaila · Enock O. Dare · Tunji J. Erinle · Olumide O. Akinpelu

Submitted: 21 August 2019 / in revised form: 8 November 2019 / Published online: 24 January 2020

Abstract Corrosion inhibition mechanisms of Rubber, Neem and Jatropha seeds oils on low-alloyed low-carbon steel in 0.5 M·H_2SO_4 environment have been investigated herein. Potentiodynamic polarization, electrochemical impedance spectroscopy and scanning electron spectroscopy techniques were employed for the experimental process. The results obtained showed that inhibition efficiencies for Rubber, Neem and Jatropha seeds oils reached values of 99.957, 99.275 and 99.998%, respectively. The most shifts in corrosion potentials were > 85 and < 85 in positive directions for Rubber and Neem seeds oils, respectively, while Gibbs free energy of adsorption had values -29.29 and -15.06 and -11.90 kJ/mol for Rubber, Neem and Jatropha seeds oils, respectively. Addition of oil inhibitors initiated formation of protective oxide films on substrate which contributed to increased inhibition efficiencies. The porosity of formed oxide film directly had impact on corrosion inhibition process as it led to localized reactions on substrate. Morphological examination of corroded substrates revealed that RSO was less prone to local corrosive attack. Inhibition efficiencies under the two electrochemical techniques employed corroborated, and corrosion inhibition occurred by retarding charge transfer reactions.

Keyword Green inhibition · Corrosion · Non-edible vegetable oils · Carbon steel · H_2SO_4

O. M. Adesusi (✉) · O. R. Adetunji · S. O. Ismaila · O. O. Akinpelu
Mechanical Engineering Department, Federal University of Agriculture, Abeokuta, Ogun State, Nigeria
e-mail: adesusiolanrewajumoses@gmail.com

E. O. Dare
Chemistry Department, Federal University of Agriculture, Abeokuta, Ogun State, Nigeria

T. J. Erinle
Mechanical Engineering Department, Federal University of Technology, Akure, Ondo State, Nigeria

Introduction

Metallic alloys on exposure to corrosive environments tend to lose their energetic state by oxidation reaction process, returning to their natural states. The oxidation reaction process is termed corrosion, which according to Adetunji et al. [1] is described as a chemical or electrochemical process involving the removal of metallic material from its bulk resulting from conversion to an oxide or other compounds. Corrosion generally reduces the useful service life of equipments as a result of inherent material loss. It has been a major topic of discussion for decades, whose effect either claimed lives or destroyed huge investments [2]. Low-alloyed low-carbon steels (LALCS) are materials of major applications in transportation, oil and gas and construction industries [3–5] such that despite their superior corrosion performance against the plain counterpart, they become degraded on exposure to aggressive media. Acid pickling and de-scaling of steel alloys, oil well acidizing and petrochemical processes [6] employ the use of acidic media such as sulfuric, nitric and hydrochloric acids, whose effects lead to oxidation of steel surfaces in contact with. As a commonly used steel de-scaling agent, Sulfuric acid is the cheapest of these mineral acids, has far lesser tendency of pitting substrates compared with hydrochloric [7] and less fuming [8]. In order to reduce effects of these acids on steel structures when used for de-scaling,

inhibitors are employed. There are other methods such as materials upgrades, production fluids blending, process controls [9], coating application and electrochemical protection [10], but inhibitors application is a cheap substitute. Synthetic corrosion inhibitors have formed a major contributor to the family of inhibitors in various applications, but pose serious environment challenge as their by-products remain non-degradable and toxic. Based on this environmental concerns, there is need to expand the frontier of green corrosion inhibitors obtained from natural sources. Besides, inhibitors are environment specific and act differently for different metallic alloys. Quite a number of researches [9, 11–15] have been conducted investigating inhibitory actions of materials of natural sources and were found to pose excellent inhibition efficiencies. Mokhtari et al. [16] extracted oil from the leaves and stems of *Jatropha curcas* and experimented the oil as inhibitor for carbon steel corrosion in 1 M HCl environment, which was found to inhibit corrosion up to 99% efficiency. Increase in the efficiency of corrosion inhibition tendency with increase in concentration of the type of vegetable oil results from the containment of C=O, oxygen, nitrogen and sulfur polar hetero-atoms or π-electrons [9, 17, 18] with multiple bonds in their molecules [19] which contribute toward inhibition by acting as the center of absorption on metal surface. The corrosion inhibition performance of Jatropha seed oil was studied on copper and its alloys and mild steel under different environments and found to have appreciable corrosion inhibition efficiencies [20]. Okewale and Olaitan [21] opined that the extract of rubber leaf is a good corrosion inhibitor for it contains phytochemicals of saponins, alkaloids, terpenes, flavonoids, glycosides, reducing sugars and tannins which was later confirmed experimentally to be true as the extract inhibited corrosion of mild steel in hydrochloric acid up to 86% efficiency obeying the Langmuir adsorption isotherm phenomenon. Mohadyaldinn et al. [22] tested the inhibition efficiency of Jatropha seeds oil on A106 carbon steel in brine and CO_2 environments using rotating cylinder electrode device and found Jatropha seed oil to inhibit corrosion. Therefore, this work investigated the corrosion inhibition mechanism of Rubber Seeds Oil (RSO), Neem Seeds Oil (NSO) and Jatropha Seeds Oil (JSO) on LALCS in H_2SO_4 environment as studies are scarcely found on this area of focus.

Materials and Methods

The materials used in this work are LALCS, Rubber, Neem and Jatropha seeds oils, H_2SO_4, grades of emery cloth, double-distilled water and acetone, while the equipment used is Optical Electron Spectroscope (OES), VersaSTAT4 potentiostat by Princeton Applied Research and Scanning Electron Spectroscope (SEM). All experiments were conducted in triplicates and parameters measured within 95% confidence interval at ambient temperature and normal pressure.

Sample Preparation and Mounting

Bulk sample of LALCS was cut into smaller samples of surface area which equaled 1.0 cm^2. These samples were mounted in epoxy resin with hardener, forming the Working Electrode (WE). Exposed surface areas of the mounted LALCS samples were abraded using emery cloth grades up to 1200, washed with double-distilled water, degreased with ethanol and acetone and dried prior to experimentation. Each sample of the WE was later connected to a three-electrode cell, run by VersaSTAT4 potentiostat of Princeton Applied Research and data acquired via Versa Studio software, alongside platinum and silver–silver chloride (Ag/AgCl) which are the counter electrode (CE) and reference electrode (RE), respectively.

Open-Circuit Potential (OCP) Determination

Open-circuit potential for each experimental run was determined by soaking the epoxy-resin-mounted samples of LALCS in the prepared 0.5 M·H_2SO_4 medium for conditions without and with oil samples of RSO, NSO and JSO in the concentration range of 0.01–0.03 g/mL. The samples soaked were allowed to corrode freely for 45 min each, until fairly steady values of potentials were achieved, without the passage of electrical current; and the potentials at which this occurred were determined through Versa Studio software before the commencement of each polarization experimental run.

Potentiodynamic Polarization (PP)

The CE, RE and WE mounted in epoxy resin were immersed into the H_2SO_4 environment without the addition of oil inhibitors. Subsequently, H_2SO_4 environment was made with the addition of RSO, NSO and JSO oil inhibitors, respectively, in concentrations that ranged 0.01–0.03 g/mL at step 0.01 g/mL. The PP corrosion tests were made positive going toward the OCP at a scan rate and potential range of 1 mV/s and ± 250 mV, respectively, for each sample prepared. Corrosion data (potential and currents) were automatically obtained via Versa Studio software, and plots of potentials against logarithm of current densities (polarization curves) were obtained alongside. The corrosion rate (CR) and inhibition efficiency (IE_{PP}) were obtained according to Eqs 1 and 2, respectively [23].

$$\mathrm{CR} = \frac{3.27 \times 10^{-3} \times i \times E_w}{d} \quad \text{(Eq 1)}$$

$$\mathrm{IE_{pp}} = \left[1 - \frac{\mathrm{CR_{inh}}}{\mathrm{CR_o}}\right] \times 100\% \quad \text{(Eq 2)}$$

where $i = \frac{I_{coor}}{A}$ (corrosion current density); A = exposed area of sample; I_{coor} = corrosion current; 3.27×10^{-3} = corrosion rate constant; E_w = sample equivalent weight; d = sample density; $\mathrm{CR_{inh}}$ = corrosion rate of sample with inhibitor; $\mathrm{CR_o}$ = corrosion rate of sample without inhibitor

Further analysis of corrosion inhibition mechanism was performed by fitting results from potentiodynamic polarization data to isotherm models, where Langmuir isotherm model was discovered to fit best. Consequently, Eq 3 [24] of Langmuir is employed. Langmuir constant K_{ads} which relates to Gibbs free energy of adsorption according to Eq 4 [12] was used to evaluate Gibbs free energy of adsorption, respectively, for RSO, NSO and JSO.

$$\theta = \frac{K_{ads}C}{1 + K_{ads}C} \quad \text{(Eq 3)}$$

$$\Delta G^{o}_{ads} = -2.303\mathrm{RT}\ \mathrm{Log}(C_{sol}K_{ads}) \quad \text{(Eq 4)}$$

where θ = adsorbate surface coverage; C = inhibitor concentration; R = 8.314 J $K^{-1}mol^{-1}$ (universal gas constant); T = 298 K (room temperature); C_{sol} = 1000 gL^{-1} (concentration of water); K_{ads} = adsorption constant (in L/g).

Electrochemical Impedance Spectroscopy (EIS)

The OCP was also determined before the EIS scan began. EIS data were obtained at a frequency range of 100 kHz to 1 Hz around the OCP and sinusoidal perturbation amplitude 10 mV (RMS). EIS data obtained were via Versa studio software which plotted both the real (Z_{re}) and imaginary (Z_{im}) parts of the impedance on x–y axes (Nyquist plots). The data were exported to EIS analysis software (EIS Spectrum Analyzer). Subsequently, Nyquist and Bode plots data were fitted to obtain semi-circles that best described each process by selecting the most suitable equivalent circuit (Fig. 1a and b) which produced the least fit errors at $< 5\%$. "NM Simp" algorithm was employed for the iteration to obtain optimal fit results. Parameters obtained from the fit results are solution resistance (R_S), LALCS Constant Phase Element ($\mathrm{CPE_{dl}}$), LALCS charge transfer resistance (R_{ct}), oxide film Constant Phase Element parameter ($\mathrm{CPE_f}$), oxide film resistance (R_f) and $\mathrm{CPE_f}$ and $\mathrm{CPE_{dl}}$ exponential factor (n). The double-layer capacitance (C_f and C_{dl}) for $\mathrm{CPE_f}$ and $\mathrm{CPE_{dl}}$ and corrosion inhibition efficiencies were calculated according to Eqs 5 [25] and 6 [12, 26].

$$C = \sqrt[n]{Y_0 \times R^{1-n}} \quad \text{(Eq 5)}$$

$$\eta = \left[1 - \frac{R^{o}_{p}}{R^{inh}_{p}}\right] \times 100\% \quad \text{(Eq 6)}$$

where $C = C_{dl}/C_f$; n = exponential factor for $\mathrm{CPE_f/CPE_{dl}}$; $Y_o = \mathrm{CPE_f/CPE_{dl}}$ values; $R_o = R_f/R_{ct}$; R^{inh}_p = polarization resistance of LALCS with inhibitor; R^{o}_p = polarization resistance of LALCS without inhibitor.

Scanning Electron Spectroscopy Examination

The surface morphologies of samples were investigated by immersing polished surface of steel samples in corrosive medium without the addition of inhibitors and with the addition of inhibitors RSO, NSO and JSO at a concentration of 0.01 g/mL, respectively. Samples were kept in this state for 2 hours after which they were extracted and dried. Subsequently, corrosion layers were examined via scanning electron microscope (SEM).

Results and Discussion

Steel Sample Composition

Elemental composition of the steel sample was determined by polishing to obtain mirror-like surface of the steel and subsequent use of Optical Electron Spectroscopy (Spark Test). The elemental composition obtained is given in Table 1.

Potentiodynamic Polarization Parameter Measurements

The corrosion parameter values for steel sample shown in Table 2 were obtained from Tafel extrapolation of polarization plots, as shown in Fig. 2, for steel sample inhibited by RSO. This table shows shifts in the corrosion potential in the more positive direction, reduction in the corrosion current densities, significant changes in both anodic and

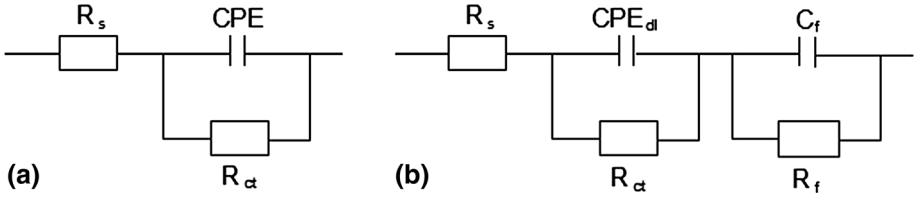

Fig. 1 EIS equivalent circuits for (**a**) uninhibited and (**b**) inhibited solutions

Table 1 Elemental composition of steel sample

Element	C	Si	Mn	P	S	Cr	Ni	Mo	Cu	Al	V	Sn
wt.%	0.0724	0.1820	0.9790	0.0102	0.0051	0.1160	0.1240	0.0425	0.2440	0.0188	0.0027	0.0087
Zn		As		Sb		Se		Te		Ta		Fe
0.0045		0.0054		0.0023		0.0031		0.0043		0.0717		Bal.

Table 2 Potentiodynamic polarization data for LALCS in 0.5 M H_2SO_4 with varying concentrations of RSO as inhibitor

RSO (g/mL)	E_{corr} (mV)	I_{corr} (nA cm^{-2})	β_a (mV/Dec)	β_c (mV/Dec)	CR × 10^{-5} (mmpy)	θ	IE_{PP} (%)
0.00	− 425.998	465,831.000	201.665	482.054	621,300.00	…	…
0.01	− 301.730	491.682	179.356	536.599	523.42	0.99916	99.916
0.02	− 273.778	225.794	209.062	636.851	270.11	0.99957	99.957
0.03	− 278.413	221.900	136.462	391.809	286.09	0.99954	99.954

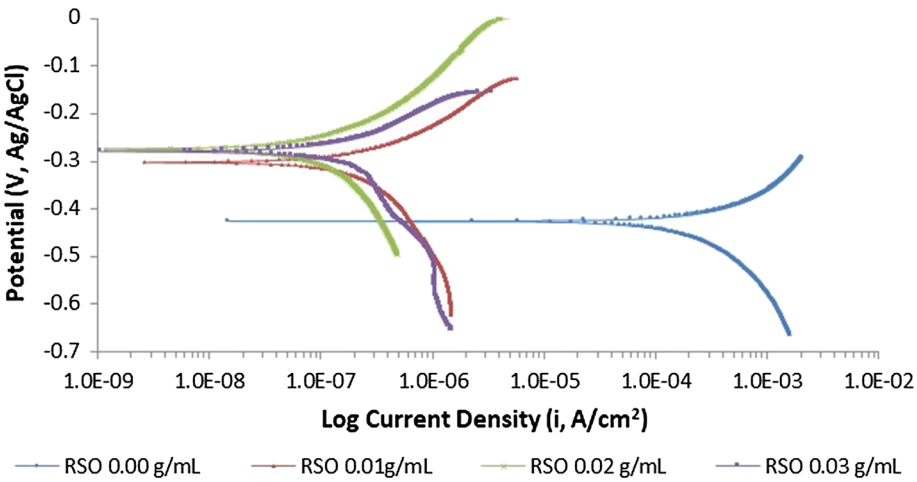

Fig. 2 Polarization curves of LALCS in 0.5 M H_2SO_4 without and with RSO as inhibitor

cathodic slope values, downward trend in the values of the corrosion rate as the concentration of RSO in the corrosive medium increased. The shifts in the corrosion potential in the more noble directions as experienced by steel sample in corrosive medium with increasing concentration of RSO are clear indications that the steel sample was rendered less susceptible to the corrosive action of the medium. This is also made evident by the downward trends of the corrosion current densities obtained and consequent increases in the inhibition efficiencies of RSO. The highest shift in corrosion potential for solution inhibited by RSO is greater than 85 mV; therefore, RSO can be classified as an anodic inhibitor. Thus, RSO inhibited corrosion of the substrate by blocking the anodic sites. Inhibition reaction of RSO was under cathodic control as the change in cathodic slopes was more significant which means the mechanism of oxidation reaction at the anodic sites was not affected, rather the hydrogen evolution mechanism at the cathode was altered by surface film formed on the substrate by RSO.

The same trend followed for the corrosion parameters in Table 3 as the corrosion potentials drifted in the nobler direction with accompanying decrease in corrosion current densities in accordance with the increase in the concentration of NSO. Nobler drift of corrosion potential showed that NSO rendered the substrate less reactive in the corrosive medium, and the highest drift in this potential was less than 85 mV which indicated mixed inhibition process which is also evident from the remarkable change in both anodic and cathodic slopes. Change in anodic and cathodic slopes showed that NSO inhibitor affected both oxidation and hydrogen evolution reactions, respectively, altering the reactions mechanism at the anodic and cathodic sites as also seen from anodic and cathodic branches of the polarization curves (Fig. 3) which seem parallel, alike and remarkably different from that without NSO. Large reduction in the anodic slope values is suggestive of increased anodic reaction due to increased anodic dissolution resulting from local action of corrosive environment.

Table 3 Potentiodynamic polarization data for LALCS in 0.5 M H_2SO_4 with varying concentrations of NSO as inhibitor

NSO (g/mL)	E_{corr} (mV)	I_{corr} (nA cm^{-2})	β_a (mV/Dec)	β_c (mV/Dec)	CR × 10^{-5} (mmpy)	θ	IE_{PP} (%)
0.00	− 425.998	465,831.000	201.665	482.054	621,300.00	…	…
0.01	− 419.582	86,920.000	39.456	146.287	92,531.00	0.85429	85.429
0.02	− 419.865	14,000.000	31.463	121.036	14,377.00	0.97686	97.686
0.03	− 399.624	3496.000	30.464	123.010	4507.40	0.99275	99.275

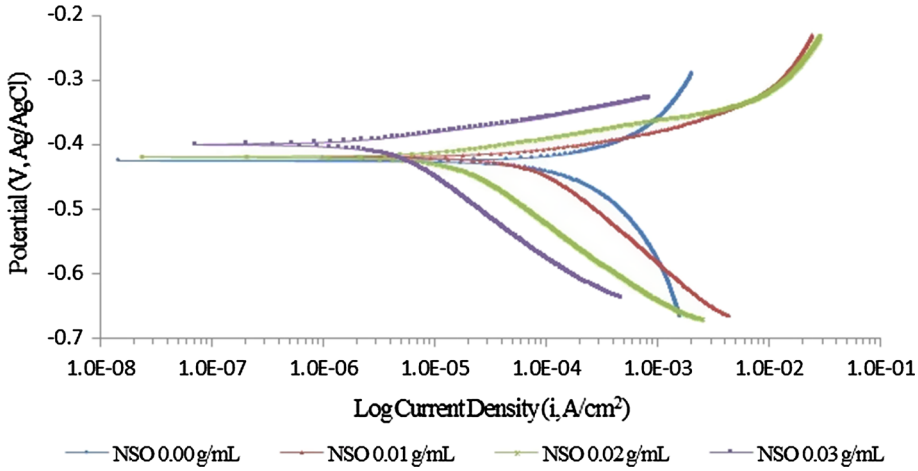

Fig. 3 Polarization curves of LALCS in 0.5 M H_2SO_4 without and with NSO as inhibitor

Table 4 Potentiodynamic polarization data for LALCS in 0.5 M H_2SO_4 with varying concentrations of JSO as inhibitor

JSO (g/mL)	E_{corr} (mV)	I_{corr} (nA cm^{-2})	β_a (mV/Dec)	β_c (mV/Dec)	CR × 10^{-5} (mmpy)	θ	IE_{PP} (%)
0.00	− 425.998	465,831.000	201.665	482.054	621,300.00	…	…
0.01	− 445.826	222,255.000	44.673	150.828	236,600.00	0.61919	61.919
0.02	− 241.272	10.380	464.325	421.556	12.42	0.99998	99.998
0.03	− 445.760	49.932	20.440	210.177	64.38	0.99990	99.990

The corrosion mechanism parameters shown in Table 4 which represent action of the corrosive medium on steel sample without and with varying concentrations of oil sample JSO give shifts of the corrosion potentials in the less noble direction (Fig. 4), except for concentration 0.02 g/mL which shifted in the positive direction. The corrosion current densities decreased, and as a result, the corrosion rate moved downward with increase in the concentration of JSO. Thus, JSO must have been adsorbed on the steel surface to have caused increase in corrosion inhibition efficiencies. Besides, both the anodic and cathodic slopes value changed significantly, altering the mechanism of reaction between the surface of the steel sample and the corrosive environment which are also evident from the change in anodic and cathodic branches of the polarization curves shown in Fig. 4.

Reduction in values of anodic slopes observed for NSO and JSO revealed an increase in the anodic current which followed that at anodic sites on the substrate there were increased reactions due to localized corrosion such as pitting or intergranular corrosion on the steel. Probable reason for the reduction in anodic slopes values may be that sulfur ligands of the inhibitor structures formed charge sharing bonds with iron resulting in weakened metal–metal bonds and subsequent lowering of the activation energy barrier responsible for metallic ions transport into corrosive solution [27] which caused severe anodic dissolution according to Eq 7 [28]. Another reason may be the porosity of protective film probably formed on substrate or interaction of inhibitor with protective layer leading to deactivation and reduction in the stability of the protective layer [29].

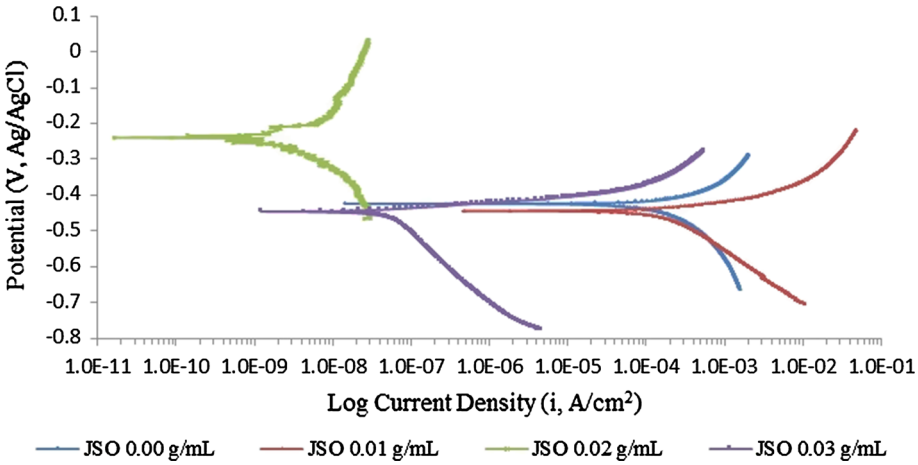

Fig. 4 Polarization curves of LALCS in 0.5 M H_2SO_4 without and with JSO as inhibitor

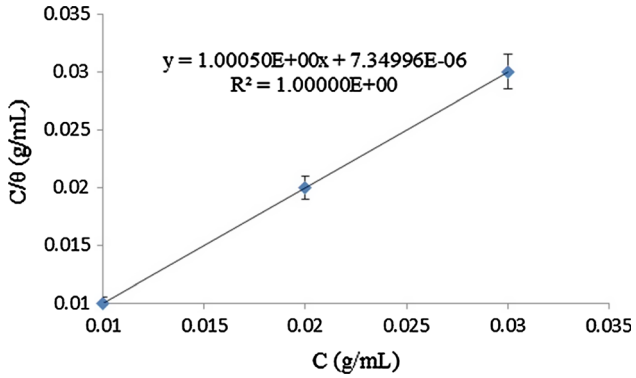

Fig. 5 Langmuir isotherm plot for substrate inhibited by RSO

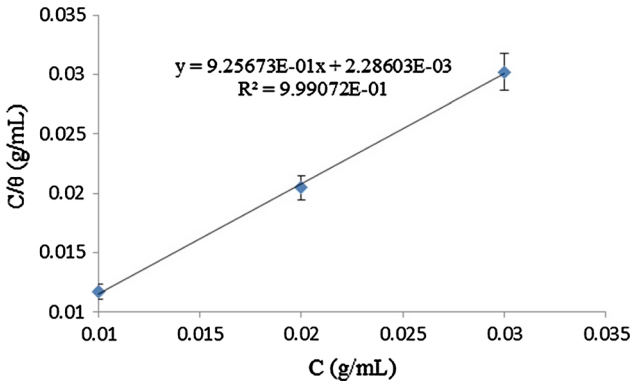

Fig. 6 Langmuir isotherm plot for substrate inhibited by NSO

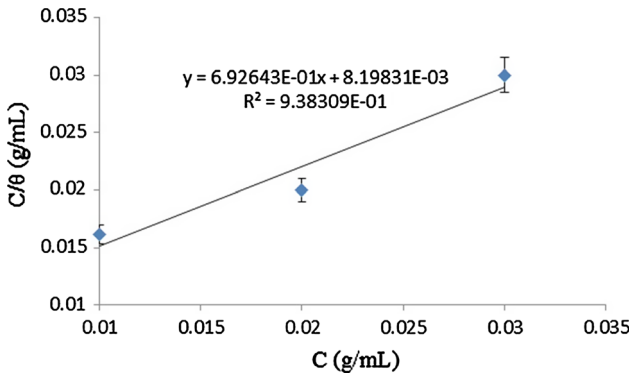

Fig. 7 Langmuir isotherm plot for substrate inhibited by JSO

$$Fe(s) + H_2SO_4(aq) \rightarrow FeSO_4(aq) + H_2(g) \quad \text{(Eq 7)}$$

Adsorption Isotherm Modeling

Data generated from Potentiodynamic Polarization test which fitted Langmuir isotherm model are shown in Figs. 5–7 for RSO, NSO and JSO, respectively. Langmuir isotherm describes interaction between molecules of inhibitors and substrate as formation of monolayer of inhibitors without lateral interaction between inhibitors molecules. Thus, all active sites are of equal energy and enthalpy of adsorption [30]. Adsorption of the inhibitors' molecules can be described as a quasi-substitution process between water molecules and inhibitor as given in Eq 8 [31], and inhibitor subsequently combined with Fe^{2+} ions to form complex as presented in Eqs 9 and 10 [32].

$$Inh_{(sol)} + mH_2O_{(ads)} \rightarrow Inh_{(ads)} + mH_2O_{(sol)} \quad \text{(Eq 8)}$$

$$Fe \rightarrow Fe^{2+} + 2e^- \quad \text{(Eq 9)}$$

$$Fe^{2+} + Inh_{(ads)} \rightarrow \left[Fe + Inh_{(ads)}\right]^{2+} \quad \text{(Eq 10)}$$

where m = size ratio.

Gibbs free energy of adsorption values for the inhibitors in Table 5 shows that the adsorption processes of inhibitors are spontaneous based on the negative values obtained. Mechanism of adsorption for RSO followed mixed adsorption process as $-20.00 > -29.29 > -40.00$ kJ mol^{-1}, while NSO and JSO followed physisorption process as both Gibbs free energy values are greater than -20.00 kJ mol^{-1}. Besides, it is worthy to note that the lesser the Gibbs free

Table 5 Langmuir isotherm data plot parameters

S/N	Experimental condition	R^2 value	Slope	Intersect	K_{ads} (mL/g)	ΔG^0_{ads} (kJ/mol)
a	Substrate in H_2SO_4 + RSO	1.0000	1.0005	7.35E−6	136054.42	− 29.29
b	Substrate in H_2SO_4 + NSO	0.9991	0.9257	2.29E−3	436.68	− 15.06
c	Substrate in H_2SO_4 + JSO	0.9383	0.6926	8.20E−3	121.95	− 11.90

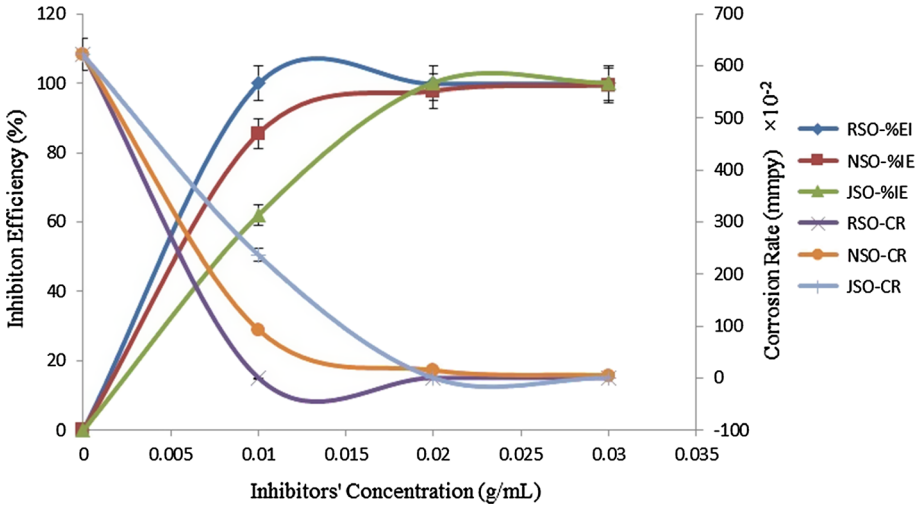

Fig. 8 Plot of corrosion rate and inhibition efficiency of RSO, NSO and JSO vs. concentration of inhibitors

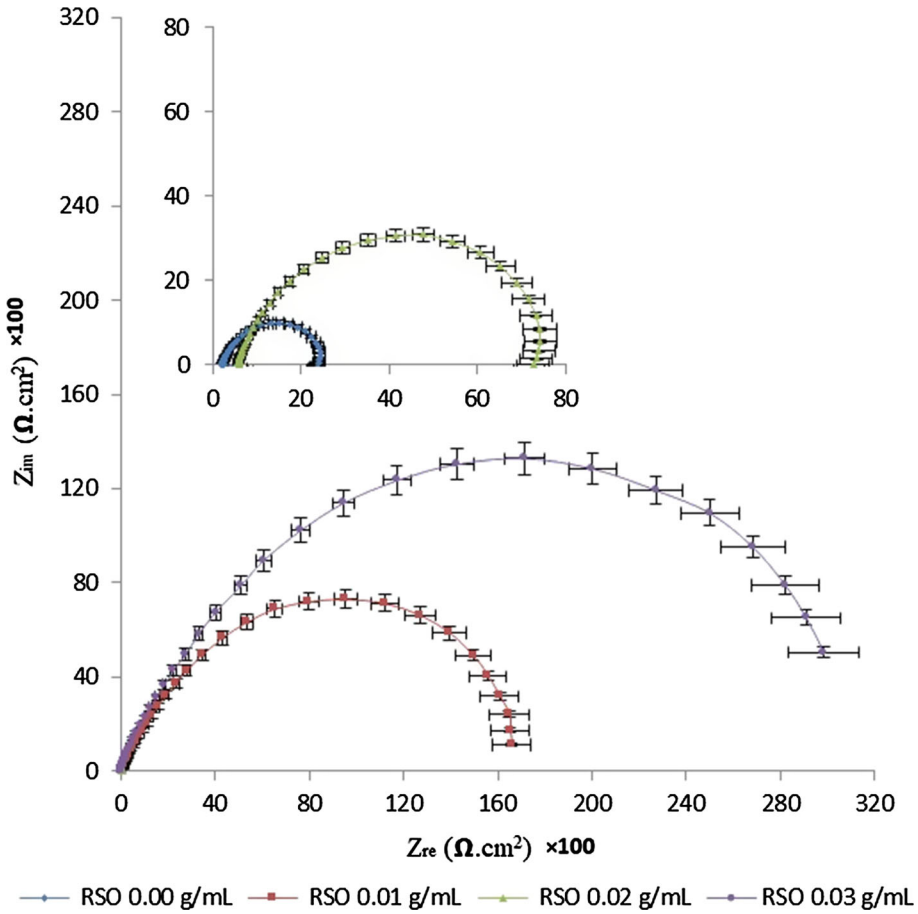

Fig. 9 Nyquist plot of steel sample in 0.5 M H_2SO_4 without and with RSO as inhibitor

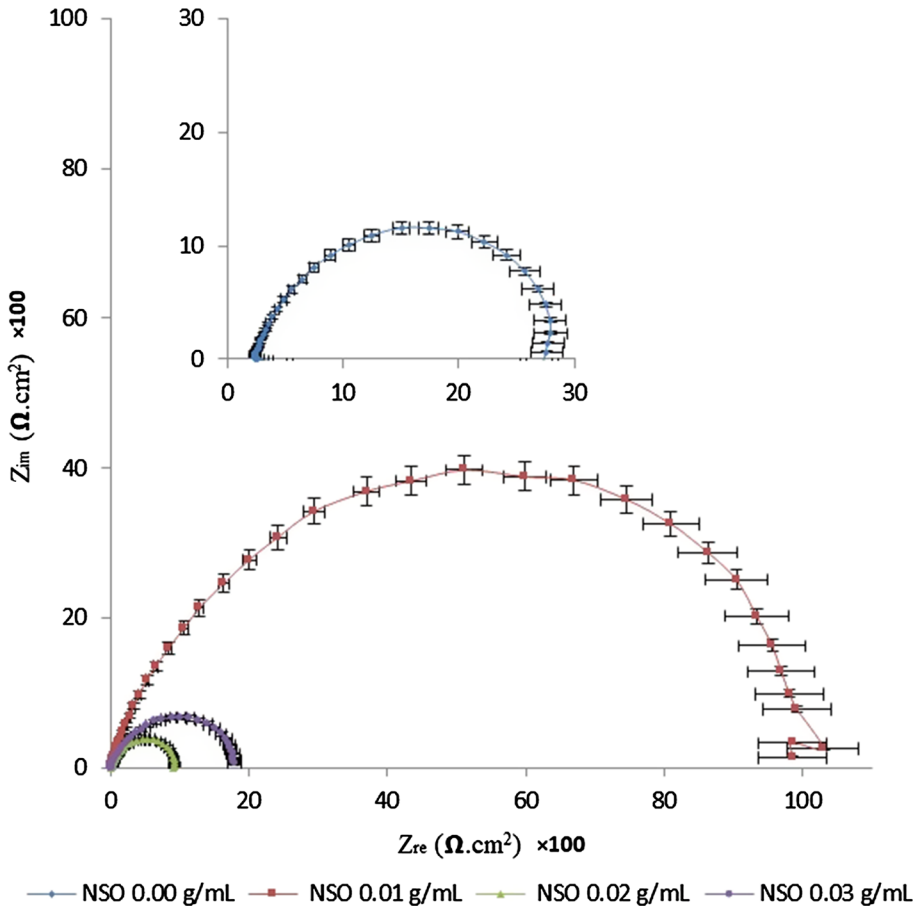

Fig. 10 Nyquist plot of steel sample in 0.5 M H_2SO_4 without and with NSO as inhibitor

energy of adsorption, the better the formation of inhibitors' film, thereby increasing the efficiency of inhibition. Therefore, RSO has the best capacity of adsorption on the substrate to form a monolayer of adsorption.

Corrosion Rate and Inhibition Efficiency of RSO, NSO and JSO

The corrosion rates of steel substrate in corrosive medium with inhibitors and inhibition efficiencies of RSO, NSO and JSO with respect to the increase in the concentration of respective inhibitor type are shown in Fig. 8. Corrosion rates are plotted on the secondary *y*-axis, while inhibition efficiencies are on the primary *y*-axis. The corrosion rates of steel substrate in corrosive medium inhibited by RSO, NSO and JSO, respectively, reduced drastically on the addition of inhibitors with corresponding increase in inhibition efficiencies. It could be seen that corrosion rate of substrate inhibited by RSO was least at concentration 0.01 g/mL and with the highest inhibition efficiency at this concentration. But as the concentrations of each inhibitor increased from 0.01 g/mL, corrosion rate of substrate inhibited by RSO increased slightly to equal corrosion rates of substrate inhibited by NSO and JSO which reduced further and with corresponding increase in inhibition efficiencies. The corrosion rate of steel substrate inhibited by RSO, which dropped slightly, may be due to the attainment of critical concentration by RSO in the corrosive medium beyond which desorption may start manifesting. Thus, at low concentration of respective inhibitor, RSO inhibited corrosion of steel substrate the best, while at higher concentrations all inhibitors are adjudged similar in inhibition efficiency.

Electrochemical Impedance Spectroscopy Parameter Measurements

Experimental outcomes from Nyquist plots shown in Figs. 9–11 display a single capacitive loop which is depressed as a result of frequency dispersion or surface heterogeneity of substrate. Larger-diameter capacitive loops were observed for substrate immersed in corrosive medium containing RSO, NSO and JSO, respectively, which corresponded to the enhanced resistance to charge transfer from steel surface into the corrosive medium.

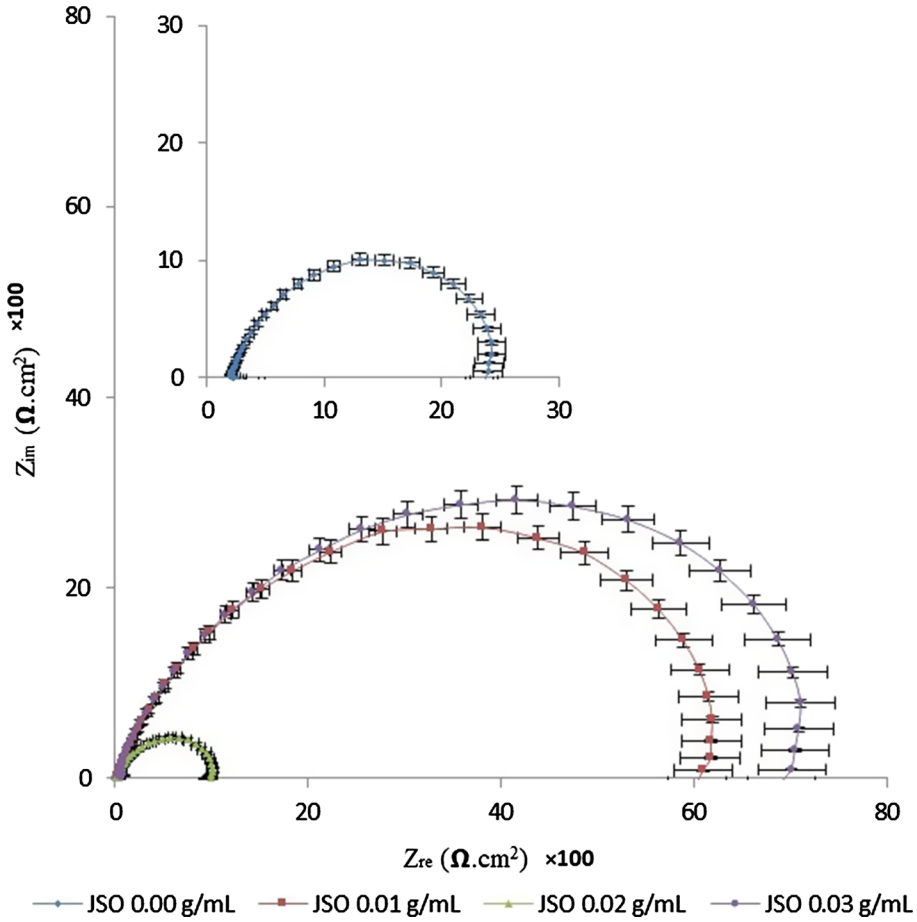

Fig. 11 Nyquist plot of steel sample in 0.5 M H_2SO_4 without and with JSO as inhibitor

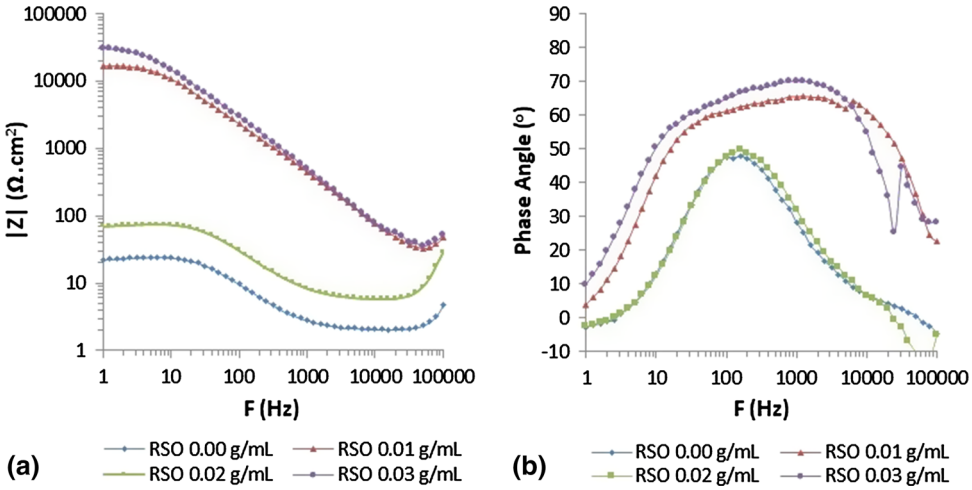

Fig. 12 Bode plot of steel sample in 0.5 M H_2SO_4 without and with RSO as inhibitor showing (**a**) impedance against frequency and (**b**) phase angle shift against frequency

The EIS parameter values measured for steel sample in corrosive medium with and without inhibitors were obtained by fitting EIS experimental values to suitable equivalent circuits. Increased impedance as shown in Figs. 12a, 13a and 14a is a result of inhibitor adsorption, limiting transportation of electrons from the substrate into corrosive medium. Steel sample immersed in corrosive medium without the addition of inhibitors showed a one-time constant feature at intermediate frequency due to single peak of phase angle, while steel samples immersed in corrosive medium with the addition of respective inhibitor at varying concentrations showed second-time constants at high-frequency regions with most phase angles at intermediate regions becoming broader [33], as shown in Figs. 12b, 13b and 14b, which are clear evidence of overlapping phase-angle peaks resulting from barrier oxide

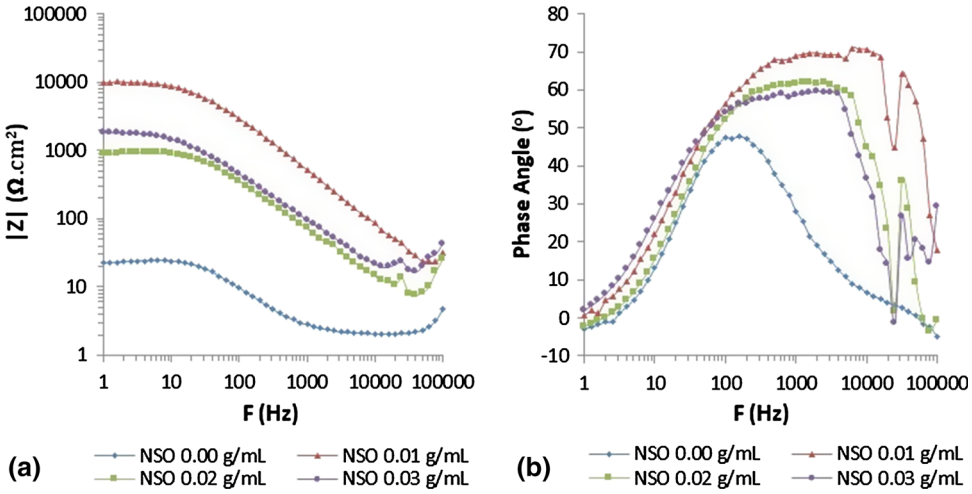

Fig. 13 Bode plot of steel sample in 0.5 M H_2SO_4 without and with NSO as inhibitor showing (**a**) impedance against frequency and (**b**) phase angle shift against frequency

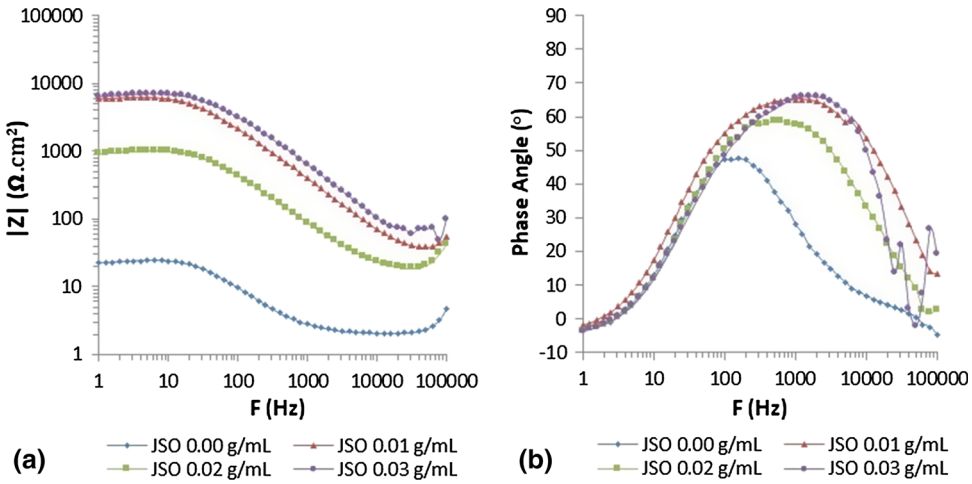

Fig. 14 Bode plot of steel sample in 0.5 M H_2SO_4 without and with JSO as inhibitor showing (**a**) impedance against frequency and (**b**) phase angle shift against frequency

film formation at the instance of inhibitors addition in the corrosive medium. Similar results were obtained by Nazari et al. [12] for Peony–Leaves-Derived Liquid used as corrosion inhibitor which enhanced formation of protective film on C1010 carbon steel in NaCl, Xu et al. [34] who used pyrazolo-pyrimidine derivative as corrosion inhibitors on copper in H_2SO_4 and Carmona-Hermandez et al. [35] where imidazole synthesized from palm oil was used as a corrosion inhibitor on supermartensitic stainless steel in H_2S, but the difference between this work and theirs is in the composition of modified Randles circuit, steel sample and type of inhibitors used.

The broad phase angles which mean that phase angle values were fairly constant over frequency ranges indicated the formation of barrier film between substrate and corrosive medium, at the instances of inhibitors addition, as shown in Fig. 15. The formed barrier film resulted from formations of complexes (oxide/barrier film) due to inhibitor/steel interaction. This indicated that the inhibition was not by mere geometric block of substrates' active sites [12]. Therefore, uninhibited solutions were modeled using simple Randles-type equivalent circuit, while inhibited solutions were modeled using the Randles-type equivalent circuit modified with two-time constant [36]. Results obtained by fitting respective equivalent circuits are shown in Tables 6, 7 and 8, where $R_p = R_{ct}$ for uninhibited solution and $R_p = R_{ct} + R_f$ for inhibited solutions. Increased values of R_p in the inhibited solutions translated to increase in inhibition efficiencies on the addition of RSO, NSO and JSO into the corrosive medium. These increases in polarization resistance resulted from effect of formed oxide film on the substrate on instances of inhibitors addition and adsorption of inhibitors at the interface between barrier film and corrosive solution.

Double-layer capacitance (C_{dl}) is related to surface area, in that the lower the capacitance, the lower will be the exposed area to corrosive solution [33]. C_{dl} values decreased on the addition of respective inhibitor, attributable to the decrease in local dielectric constant or increase in thickness of electrical double layer resulting

from adsorption of inhibitor molecules at interface between steel and corrosive medium [15], showing that the adsorption of inhibitors which introduced barrier film covering surface area of substrate made it less available for corrosive attacks. Increased values of C_f, C_{dl} and decreased values of R_f, R_{ct} as the inhibitors' concentrations changed from 0.01 to 0.03 g/mL in certain instances, i.e., concentration 0.02 g/mL of RSO, are clear indication of the porous nature of barrier film which allowed the corrosive medium to seep through it causing localized attacks on the substrate. These are likely due to low solubility of oil inhibitors and its interaction with protective oxide layer leading to instability of protective layer and subsequent deactivation of inhibitors' molecules [29]. The increase in values of C_f and C_{dl} for NSO was steady with the increase in its concentration, which may mean that the increase in its concentration led to the increased deactivation and porosity of the oxide layer. Inhibition efficiencies of the oil inhibitors which reached minimum 64.42% were due to oxide layer (R_f) and charge transfer (R_{ct}) resistances. The difference in values of inhibition efficiencies between the two electrochemical techniques may be attributed to the presence of charged particles in the oil samples or steel sample surface alteration due to polarization.

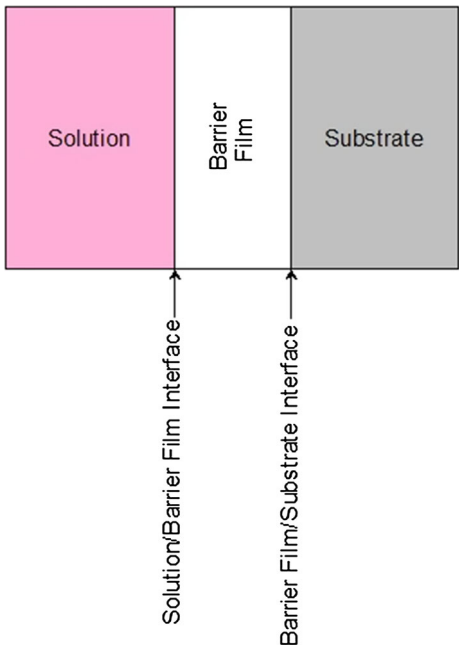

Fig. 15 Schematic of substrate in H_2SO_4 with the addition of inhibitors introducing barrier film at solution/substrate interface

Scanning Electron Spectroscopy Surface Morphology Examination of Immersed Sample

The micrographs displayed in Fig. 16a and d show the morphologies of the steel sample immersed in H_2SO_4 without the addition of oil, with additions of RSO, NSO and JSO, respectively. Figure 16a is characterized with denser product corrosion formed on the steel surface resulting from the action of the corrosive medium. Conversely, Fig. 16b and c indicates less corrosion product formed on the steel surface but with micro-pits, especially on sample inhibited by NSO. Figure 16d in its own case is

Table 6 EIS data fit result for LALCS in 0.5 M H_2SO_4 with varying concentration of RSO as inhibitor

	CPE_f				CPE					
RSO (g/mL)	$Y_o \times 10^{-6}$ (s^n/Ω cm^2)	n	R_f (Ω cm^2)	C_f (μF/cm^2)	$Y_o \times 10^{-6}$ (s^n/Ω cm^2)	n	R_{ct} (Ω cm^2)	C_{dl} (μF/cm^2)	R_p (Ω.cm^2)	IE_{EIS} (%)
0.00	…	…	…	…	404.290	0.8551	24.13	184.47	24.13	…
0.01	4.10	0.7704	1257.20	0.85	1.51	0.9327	15869.00	1.15	17126.20	99.86
0.02	308.00	0.8004	10.54	73.78	72.40	1.0000	57.28	72.40	67.82	64.42
0.03	2.61	0.7956	4729.10	0.84	1.22	1.0000	25639.00	1.22	30368.10	99.92

Table 7 EIS data fit result for LALCS in 0.5 M H_2SO_4 with varying concentrations of NSO as inhibitor

	CPE_f				CPE					
RSO (g/mL)	$Y_o \times 10^{-6}$ (s^n/Ω cm^2)	n	R_f (Ω cm^2)	C_f (μF/cm^2)	$Y_o \times 10^{-6}$ (s^n/Ω cm^2)	n	R_{ct} (Ω cm^2)	C_{dl} (μF/cm^2)	R_p (Ω cm^2)	IE_{EIS} (%)
0.00	…	…	…	…	404.290	0.8551	24.13	184.47	24.13	…
0.01	2.04	0.8082	3192.60	0.62	1.26	0.9962	6717.60	1.24	9910.20	99.76
0.02	6.63	0.9297	59.65	3.67	7.06	0.9326	857.45	2.02	917.10	97.37
0.03	9.10	0.8838	117.65	3.70	9.70	0.8703	1688.80	5.26	1806.45	98.66

Table 8 EIS data fit result for LALCS in 0.5 M H_2SO_4 with varying concentrations of JSO as inhibitor

RSO (g/mL)	CPE_f		R_f (Ω cm^2)	C_f (μF/cm^2)	CPE		R_{ct} (Ω cm^2)	C_{dl} (μF/cm^2)	R_p ($\Omega.cm^2$)	IE_{EIS} (%)
	$Y_o \times 10^{-6}$ (s^n/Ω cm^2)	n			$Y_o \times 10^{-6}$ (s^n/Ω cm^2)	n				
0.00	…	…	…	…	404.290	0.8551	24.13	184.47	24.13	…
0.01	3.11	0.8118	920.07	0.80	1.14	0.9787	5227.3	1.02	6147.37	99.61
0.02	18.00	0.8482	137.46	6.15	4.87	1.0000	761.36	4.87	898.82	97.32
0.03	0.56	0.9860	569.41	0.50	0.71	0.9325	6561.10	0.48	7130.51	99.66

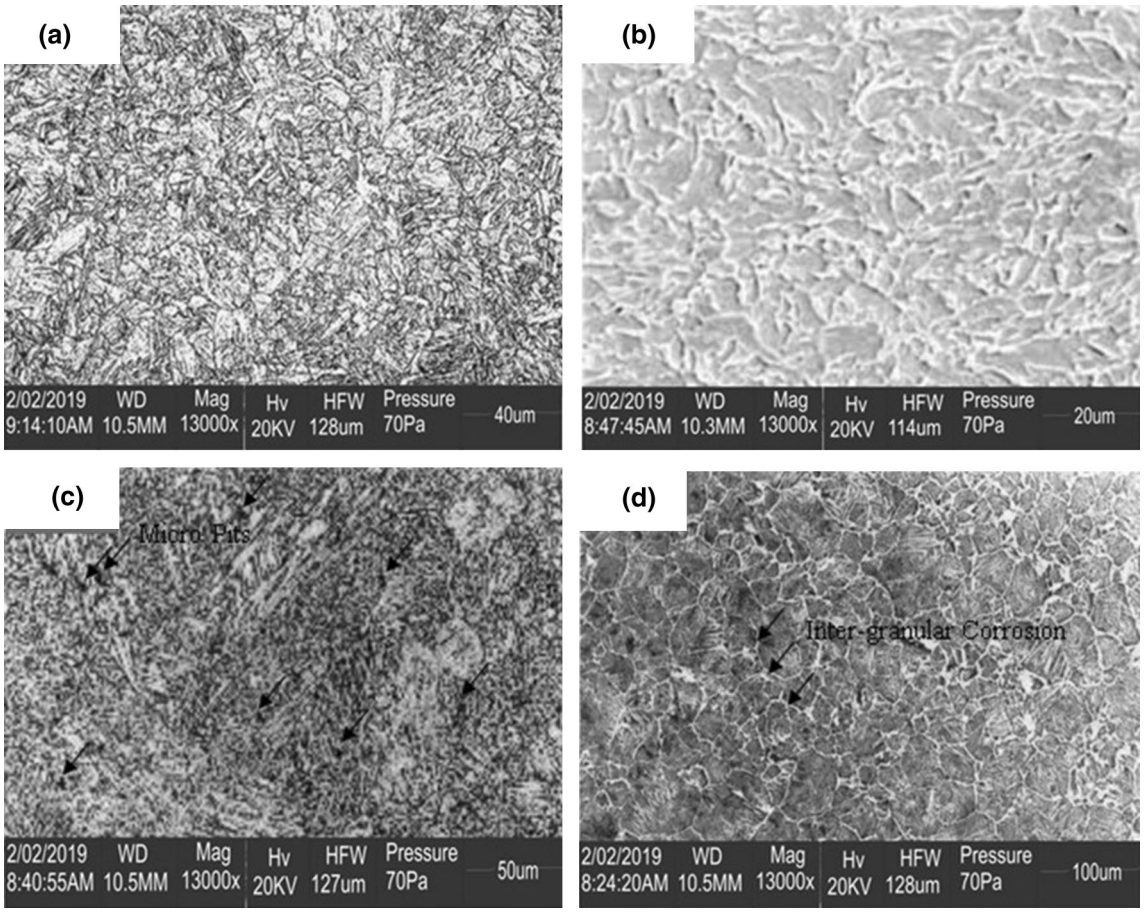

Fig. 16 SEM micrograph of steel sample after 2-h immersion in (**a**) H_2SO_4 (**b**) H_2SO_4 + RSO (**c**) H_2SO_4 + NSO (**d**) H_2SO_4 + JSO

characterized with the corrosion product formation on the grain boundary with no visible formation of corrosion on the grain face. Surface morphologies via SEM vividly support the results obtained for potentiodynamic polarization and electrochemical impedance spectroscopy. Denser corrosion product on the sample without any of the RSO, NSO and JSO evidently showed that the oil sample inhibited corrosion of the steel sample in the corrosive medium. Micro-pits and mild intergranular corrosion seen on the morphologies obtained from samples inhibited by RSO, NSO and JSO, respectively, are likely due to local actions of sulfur ligands contained in the oil samples or corrosive medium sipping through the pores of barrier films formed, which are also indicative of reasons for the reduction in both the anodic and cathodic Tafel slopes obtained for NSO and JSO.

Conclusion

The corrosion inhibition mechanisms of RSO, NSO and JSO have been studied and result presented. Based on the results, the following conclusions are drawn:

- RSO, NSO and JSO inhibited LALCS in H_2SO_4 effectively, especially generation corrosion.
- RSO exhibited anodic corrosion inhibition feature, NSO in its own case exhibited mixed corrosion inhibition feature, while JSO could not be classified.
- Adsorption mechanisms of RSO, NSO and JSO obeyed Langmuir adsorption isotherm model and were spontaneous.
- Adsorption of RSO on substrate was by electrostatic interaction and chemical reaction between inhibitor and substrate (mixed adsorption), while adsorption of NSO and JSO was mainly by electrostatic interaction between inhibitors and substrate (physisorption).
- The best inhibition efficiency was obtained using RSO at lower concentration, while at higher concentration inhibition efficiencies for RSO, NSO and JSO reached the same values.
- Based on the Gibbs free energy of adsorption values, RSO poses the strongest and most stable adsorption on LALCS.
- Addition of RSO, NSO and JSO, respectively, caused the formation of barrier film on the substrate in the corrosive medium, contributing to increased charge transfer resistance and corrosion inhibition process.
- Barrier film formed confirmed that the inhibition process was not controlled by geometric blocking of active site but as a result of complexes formed.
- Localized corrosive attack on the anodic site is not as clearly defined on solutions inhibited by RSO compared with that inhibited by NSO and JSO, judging from the morphological examination and decrease in the anodic slopes. Therefore, RSO inhibited general and localized corrosion more effectively.
- Localized attacks are likely due to activities of sulfur ligands in oil inhibitors or corrosive medium seeping through the porous layer of protective oxide films.

Acknowledgments The authors wish to express their profound gratitude to MIDWAL engineering, Lagos, Nigeria, and Department of Metallurgical and Materials Engineering, Federal University of Technology, Akure, Nigeria, for use of equipment and facilities in the course of the experimental work.

References

1. O.R. Adetunji, P.O. Aiyedun, O.J. Alamu, A.S. Surakat, Electrochemical properties of metals in cassava fluid. J. Eng. Technol. Res. **3**(10), 292–297 (2011)
2. O.A. Omotosho, J.O. Okeniyi, J.O. Ikotun, C.A. Loto, A.P.I. Popoola, Corrosion behaviour of mild steel in 0.5 M sulphuric acid media in the presence of potassium chromate. J. Eng. Appl. Sci. **13**(14), 5789–5795 (2018)
3. V.I. Astaschenko, E.A. Zapadnova, N.N. Zapadnova, G.F. Mukhametzyanova, Predicting structure micro-alloyed steel products of different purpose. IOP Conf. Ser. Mater. Sci. Eng. **134**, 1–3 (2016)
4. S.S. Rawat, M.K. Sharma, M.S. Gurjar, Investigation on trip behaviour of low carbon micro alloyed steel. Inter. J. Eng. Technol. Sci. Res. **3**(5), 25–33 (2016)
5. Y. Tian, H. Wang, Y. Li, Z. Wang, G. Wang, The analysis of the microstructure and mechanical properties of low carbon microalloyed steels after ultra fast cooling. Mater. Res. **20**(3), 853–859 (2017)
6. M. Faisal, A. Saeed, D. Shahzad, N. Abbas, F.A. Larik, General properties of and comparison of the corrosion inhibition efficiency of the triazole derivatives for mild steel. Corros. Rev. **36**(6), 507–545 (2018)
7. American Iron and Steel Institute, A Designers' Handbook Series N^o 9001: Cleaning and Descaling Stainless Steels. Nickel Development Institute. North Carolina, USA. 36pp (1988) (Original Work Published 1982)
8. L. Messaadia, O.I.D. El Mouden, A. Anejjar, M. Messali, R. Salghi, O. Benali, O. Cherkaoui, A. Lallam, Adsorption and corrosion inhibition of new synthesized pyridazinium-based ionic liquid on carbon steel in 0.5 M H_2SO_4. J. Mater. Environ. Sci. **6**(2), 598–606 (2015)
9. M.S. Al-Otaibi, A.M. Al-Mayouf, M. Khan, A.A. Moussa, S.A. Al-Mazroa, H.Z. Alkhathlan, Corrosion inhibitory action of some plant extracts on the corrosion of mild steel in acidic media. Arab. J. Chem. **7**, 340–346 (2014)
10. G. Aziate, A. El Yadini, H. Saufi, A. Almaofari, A. Benhmama, H. Harhar, S. Gharby, S. El Hajjaji, Study of jojoba vegetable oil as inhibitor of carbon steel C38 corrosion in different acidic media. J. Mater. Environ. Sci. **6**(7), 1877–1884 (2015)
11. A.S. Yaro, A.A. Khadom, R.K. Wael, Apricot juice as green corrosion inhibitor of mild steel in phosphoric acid. Alexandria Eng. J. **52**, 129–135 (2013)
12. M.H. Nazari, M.S. Shihab, L. Cao, E.A. Haven, X. Shi, A peony–leaves-derived liquid corrosion inhibitor: protecting carbon steel form NaCl. Green Chem. Lett. Rev. **10**(4), 359–379 (2017)
13. N. Belarbi, F. Dergal, I. Chikhi, S. Merah, D. Lerari, K. Bachari, Study of anti-corrosion activity of *Algerian* L. stoechas oil on C38 carbon steel in 1 M HCl medium. Int. J. Ind. Chem. **9**(2), 115–125 (2018)
14. M. Zouarhi, M. Chellouli, S. Abbout, H. Hammouch, A. Dermaji, S.O. Said Hassane, P. Decaro, N. Bettach, N. Hajjaji, A. Srhiri, Inhibiting effect of a green corrosion inhibitor containing *Jatropha curcas* seed oil for iron in an acidic medium. Portugaliae Electrochimi Acta **36**(3), 179–195 (2018)
15. K. Chatoui, S. Echihi, H. Harhar, A. Zarrouk, M. Tabyaoui, An investigation of carbon steel corrosion inhibition in 1 M HCl by *Lepidium sativum* oil as green inhibitor. J. Mater. Environ. Sci. **9**(4), 1212–1223 (2018)
16. O. Mokhtari, I. Hamdani, A. Chetouani, A. Lahrach, A. ElHalouani, A. Aounit, M. Berrabah, Inhibition of steel corrosion in 1 M HCl by *Jatropha curcas* Oil. J. Mater. Environ. Sci. **5**(1), 310–319 (2014)
17. V.M. Abbasov, I.T. Ismayilov, H.M. Abd El-Lateef, S.F. Akhmadbeyovea, Anti-corrosive activities of some novel surfactants based on vegetable oils. Eur. Chem. Bull. **3**(5), 437–440 (2014)
18. S.O. Ajeigbe, N. Basar, M.A. Hassan, M. Aziz, Optimization of corrosion inhibition of essential oils of *Alpina galanga* on mild steel using response surface methodology. ARPN J. Eng. Appl. Sci. **12**(9), 2763–2771 (2017)
19. B.U. Ugi, T.O. Magu, Inhibition, adsorption and thermodynamic investigation of iron corrosion by green inhibitors in acidic medium. Int. J. Sci. Technol. **5**(4), 56–64 (2017)
20. S. Aribo, O.J. Samuel, S.J. Olusegun, A.S. Ogunbadejo, O.O. Ige, *Jatropha curcas* as a corrosion inhibitor for API 5L-X65 steel

under sand deposit in CO_2 and aerated oil field environments. Afr. Corros. J. **2**(2), 17–27 (2016)
21. A.O. Okewale, A. Olaitan, The use of rubber leaf extract as a corrosion inhibitor for mild steel in acidic solution. Inter. J. Mater. Chem. **7**(1), 5–12 (2017)
22. M.E. Mohadyaldinn, N. Azad, A.K. Azad, Evaluation of *Jatropha curcas* oil as corrosion inhibitor of CO_2 corrosion in petroleum production environment. J. Appl. Environ. Biol. Sci. **7**(35), 28–34 (2017)
23. R.T. Loto, Corrosion polarization behaviour and inhibition of S40977 stainless steel in benzosulfonazole/3M H_2SO_4 solution. S. Afr. J. Chem. Eng. **24**, 148–155 (2017)
24. E. Ituen, O. Akaranta, A. James, Evaluation of performance of corrosion inhibitors using adsorption isotherm models: an overview. Chem. Sci. Inter. J. **18**, 1–34 (2017)
25. A. Chaouiki, H. Lgaz, R. Salghi, S.L. Gaonkar, K.S. Bhat, S. Jodeh, K. Toumiat, H. Oudda, New benzohydrazide derivative as corrosion inhibitor for carbon steel in a 1.0 M HCl solution: electrochemical, DFT and Monte Carlo simulation studies. Portugaliae Electrochimi. Acta **37**(3), 147–165 (2019)
26. A. Singh, M. Talha, X. Xu, Z. Sun, Y. Lin, Heterocyclic corrosion inhibitors for J55 steel in a sweet corrosive medium. ACS Omega **2**, 8177–8186 (2017)
27. A. Kosari, M.H. Moayed, A. Davoodi, R. Parvizi, M. Momeni, H. Eshghi, H. Moradi, Electrochemical and quantum chemical assessment of two organic compounds from pyridine derivatives as corrosion inhibitors for mild steel in HCl solution under stagnant condition and hydrodynamic flow. Corros. Sci. **78**, 138–150 (2014)
28. R.T. Loto, Electrochemical analysis of the corrosion inhibition properties of L-leucine and trypsin complex admixture on high carbon steel in 1 M H_2SO_4 solution. Rev. Colomb. Quim. **47**(2), 12–20 (2018)
29. M. Taghavikish, N.K. Dutta, N.R. Choudhury, Emerging corrosion inhibitors for interfacial coating. Coatings **7**, 1–28 (2017)
30. M. Butnariu, P. Negrea, L. Lupa, M. Ciopee, A. Negrea, M. Pentea, I. Sarac, I. Samfira, Remediation of rare earth element pollutants by sorption process using organic natural sorbents. Inter. J. Environ. Res. Public Health **12**, 11278–11287 (2015)
31. V.M. Abbasov, H.M. Abd El-Lateef, L.I. Aliyeva, E.E. Qasimov, I.T. Ismayilov, M.M. Khalaf, A study of the corrosion inhibition of mild steel C1018 in CO_2-saturated brine using some novel surfactants based on corn oil. Egypt. J. Pet. **22**, 451–470 (2013)
32. M.Y. Diaz-Cardenas, M.G. Valladares-Cisneros, S. Lagunas-Rivera, V.M. Salinas-Bravo, R. Lopez-Sesenes, J.G. Gonzalez-Rodriguez, Peumus boldus extract as corrosion inhibitor for carbon steel in 0.5 M sulfuric acid. Green Chem. Lett. Rev. **10**(4), 257–268 (2017)
33. Q. Wang, J. Yu, J. Xu, H. Fang, S. Liu, Y. Tang, Y. Xi, S. Bai, Realization of graphene on the surface of electroless Ni–P coating for short-term corrosion prevention. Coatings **130**(8), 1–10 (2018)
34. Y. Xu, S. Zhang, W. Li, L. Guo, S. Xu, L. Feng, L.H. Madkour, Experimental and theoretical investigations of some pyrazolo–pyrimidine derivatives as corrosion inhibitors on copper in sulfuric acid solution. Appl. Surf. Sci. **459**, 612–620 (2018)
35. A. Carmon-Hernandez, E. Vazquez-Velez, J. Uruchurtu-Chavarin, J.G. Gonzalez-Rodriguez, L. Martinez-Gomez, Use of an imidazol synthetized from palm oil as corrosion inhibitor for a supermartensitic stainless steel in H_2S. Green Chem. Lett. Rev. **12**(1), 89–99 (2019)
36. D.V. Ribeiro, C.A.A. Souza, J.C.C. Abrantes, Use of electrochemical impedance spectroscopy (EIS) to monitoring the corrosion of reinforced concrete. Ibracon Struct. Mater. J. **8**(4), 529–546 (2015)